SANDIA REPORT
SAND2020-9842
Printed September 2020

Sandia National Laboratories

Coupling CTH to Linear Acoustic Propagation across an Air-Earth Interface

Leiph A. Preston, Mehdi Eliassi, and Christian Poppeliers

Prepared by
Sandia National Laboratories
Albuquerque, New Mexico
87185 and Livermore,
California 94550

Issued by Sandia National Laboratories, operated for the United States Department of Energy by National Technology & Engineering Solutions of Sandia, LLC.

Available to DOE and DOE contractors from
U.S. Department of Energy
Office of Scientific and Technical Information
P.O. Box 62
Oak Ridge, TN 37831

Telephone: (865) 576-8401
Facsimile: (865) 576-5728
E-Mail: reports@osti.gov
Online ordering: http://www.osti.gov/scitech

Available to the public from
U.S. Department of Commerce
National Technical Information Service
5301 Shawnee Rd
Alexandria, VA 22312

Telephone: (800) 553-6847
Facsimile: (703) 605-6900
E-Mail: orders@ntis.gov
Online order: https://classic.ntis.gov/help/order-methods/

ABSTRACT

The interface between the Earth and the atmosphere forms a strong contrast in material properties. As such, numerical issues can arise when simulating an elastic wavefield across such a boundary when using a numerical simulation scheme. This is exacerbated when two different simulation codes are coupled straddling that interface. In this report we document how we implement the coupling of CTH, a nonlinear shock physics code, to a linearized elastic/acoustic wave propagation algorithm, axiElasti, across the air-earth interface. We first qualitatively verify that this stable coupling between the two algorithms produces expected results with no visible effects of the coupling interface. We then verify the coupling interface quantitatively by checking consistency with results from previous work and with coupled acoustic-elastic seismo-acoustic source inversions in three earth materials.

ACKNOWLEDGEMENTS

This research was funded by the National Nuclear Security Administration, Defense Nuclear Nonproliferation Research and Development (NNSA DNN R&D). The authors acknowledge important interdisciplinary collaboration with scientists and engineers from LANL, LLNL, MSTS, PNNL, and SNL. This paper describes objective technical results and analysis. Any subjective views or opinions that might be expressed in the paper do not necessarily represent the views of the U.S. Department of Energy or the United States Government.

CONTENTS

LIST OF FIGURES

LIST OF TABLES

This page left blank

ACRONYMS AND DEFINITIONS

Abbreviation	Definition
2D-C	two dimensional cylindrical
TVBC	time varying boundary condition
2-C	two component
MPa	megapascal
Nm	Newton-meters
Vp	P-wave velocity
Vs	S-wave velocity

1. INTRODUCTION

Buried explosions nonlinearly deform the surrounding earth, causing fracturing and plastic deformation of the material. For shallowly buried explosions, the nonlinear zone can extend to the Earth's surface, cause blow out and cratering, and induce a nonlinear acoustic wave in the atmosphere. For intermediately buried explosions, the earth material near the surface can be nonlinearly deformed, but still produce an acoustic wave that is very closely approximated as linear. Due to the decrease in lithostatic stresses as one approaches the surface from below coupled with the fact that weaker, weathered materials such as soils are typically present at the Earth's surface, the explosion could produce two zones of nonlinear deformation: the usual nonlinear zone centered on the explosion point itself, plus another near the surface, separated by a region of deformation that is approximately linear.

In cases where the earth behaves weakly nonlinear at the surface, meaning no macroscopically visible signs of nonlinear deformation such as cratering occurs, the nonlinear deformation at the Earth's surface could still induce an acoustic wave into the atmosphere that would not follow strictly linear acoustic transmission across that interface. To simulate the explosion-induced wavefield in these cases, it would be advantageous to couple the results of the nonlinear calculation to the input of a linear propagation code as close to the Earth's surface as possible. This allows capturing of all the near-surface nonlinear effects within the earth while still availing ourselves of the more computationally efficient linear wave propagation algorithms. However, the approximately factor of 1000 difference between air and typical rock densities along with the strong contrast in both linear and nonlinear material properties can cause numerical issues at this boundary (Preston et al., 2008). These potential issues must be addressed before a stable and accurate coupling interface between the codes can be accomplished.

The nonlinear code we use in this report is Sandia's CTH (Schmitt et al., 2017), a shock physics algorithm capable of computing nonlinear effects, such as plastic deformations and fracturing. The linear elastic/acoustic wave propagation code we will be using is axiElasti (Preston, 2017). The Preston (2017) report describes the 2-D cylindrical (2DC) elastic wave propagation algorithm itself, plus it documents the coupling of 2DC CTH runs to axiElasti when in a homogeneous earth material (i.e. no air layer).

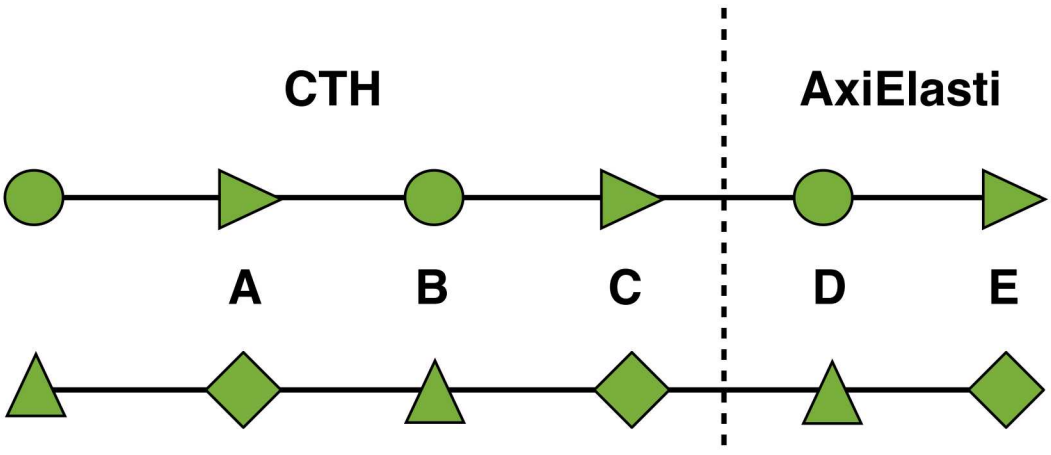

Figure 1-1: Required spatial distribution of velocities (triangles), compressive stresses (circles), and shear stresses (diamonds) needed by axiElasti from the CTH domain for time varying boundary conditions. Distance between A and C is *dh*.

Although the details are provided in the Preston (2017) report, a brief overview here will be useful. axiElasti solves the velocity-stress coupled set of partial differential equations using second order temporally and fourth order spatially accurate finite-difference operators. In order to implement time-varying boundary conditions (TVBC) for axiElasti and due to the fourth order spatial accuracy of its operators, a TVBC box with thickness dh (axiElasti node spacing) which completely surrounds the source is required. This box is discretized so that it aligns with the axiElasti grid and these points form tracers, which are where CTH records all components of velocities and stresses for all times in its simulation. These points then can act as TVBC that drive axiElasti propagation (Figure 1-1). In order to compute point D from Figure 1-1 in axiElasti, the staggered grid stencil needs information from CTH at points A and C. Likewise, to compute point E in axiElasti we need information from point B in CTH (in addition to point D, which is computed by axiElasti directly). This is a one-way coupling only: no information passes back to CTH from the axiElasti domain.

Within a homogeneous medium, as long as the edges of the TVBC box are beyond the elastic radius for the simulated explosion, the precise locations of the TVBC edges relative to CTH element boundaries are unimportant. However, for a layered structure, questions arise such as how the CTH elements should be aligned relative to the layer interfaces, how the TVBC points should be aligned relative to both the CTH elements and layer interfaces, and how specific nonlinear material properties at the interface affect the TVBC accuracy. We explore these questions in this report using a model with air over a single layer of homogeneous basalt, salt, or wet tuff and then demonstrate the validity of our approach with some test cases.

2. IMPLEMENTATION

We will first describe the baseline model used in this section, then briefly describe issues that arose in our initial attempts at coupling CTH and axiElasti across the air-earth interface. Finally, we will outline the method we found that produces stable and accurate simulations across the air-earth interface.

2.1. Basic Model Setup

The basic model setup is the same for all cases in this section unless specifically mentioned otherwise. Basalt (seslan number 7530 from SESAME tables: Kerley and Christian-Frear 1993) was used as the homogeneous earth material for CTH simulations. As described in Preston (2017), elastic equivalent parameters (P-wave velocity (Vp) = 7030 m/s, S-wave velocity (Vs) = 4059 m/s, and density = 2868 kg/m^3) for the basalt were used in the axiElasti simulations. We modeled air as an ideal gas within CTH, and with elastic parameters Vp=340 m/s, Vs = 1e-6 m/s, and density = 1.2 kg/m^3 within axiElasti. A small but non-zero Vs is used for air in axiElasti to avoid numerical errors that would be present for Vs precisely equal to zero. The 2-D cylindrical coordinate system is designed so that z=0 m is the interface between air and basalt and positive z points upward and x=0 m is the symmetry axis. A 4.5 kg TNT explosion is simulated in CTH at a depth of 10 m (z=-10 m) within the basalt (scaled depth of burial ~481 m/kt$^{1/3}$). The explosion is modeled using Jones-Wilkins-Lee (JWL) programmed burn for TNT with the default parameters as provided in CTH (Schmitt et al., 2017). Tracers are placed at roughly 11 m from the source: r = 11 m between z=-21 m and z=1 m and at z=-21 m and at z=1 m from r=0 m to r=11 m (Figure 2-1). Note that the top tracers are placed 1 m above the interface in air. Based on the frequency content desired for the axiElasti simulations, dh=14 cm was used in the axiElasti simulations and between tracer points used in CTH to capture the TVBC. The CTH simulation was stopped at 0.05 s after detonation of the explosive. A 240 Hz low pass filter was applied to output CTH tracer data prior to input into axiElasti as TVBC.

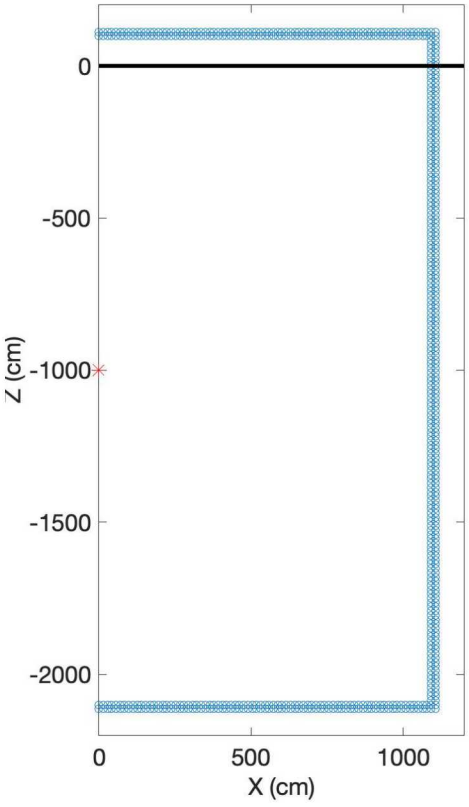

Figure 2-1: Basic model setup. The source point (red star) is surrounded by tracer points (blue circles) at roughly 11 m from the source. The air-earth interface is given by the black line at z = 0 m. Air is above, basalt below.

2.2.Initial Issues

When we first attempted the basic model setup as described above, multiple issues were discovered (Figure 2-2). One of the obvious problems with this model is the energy emanating from the corner where the TVBC box intersects the air-earth interface. This high-amplitude, high-frequency extraneous source produces noise that swamps any valuable waveform data near this corner that propagates at the speed of sound outward. A second major issue is the orders of magnitude higher amplitude of the upward traveling acoustic wave directly above the CTH domain compared to that which is dominated by elastic-acoustic conversion within axiElasti itself at larger distances. The spurious corner

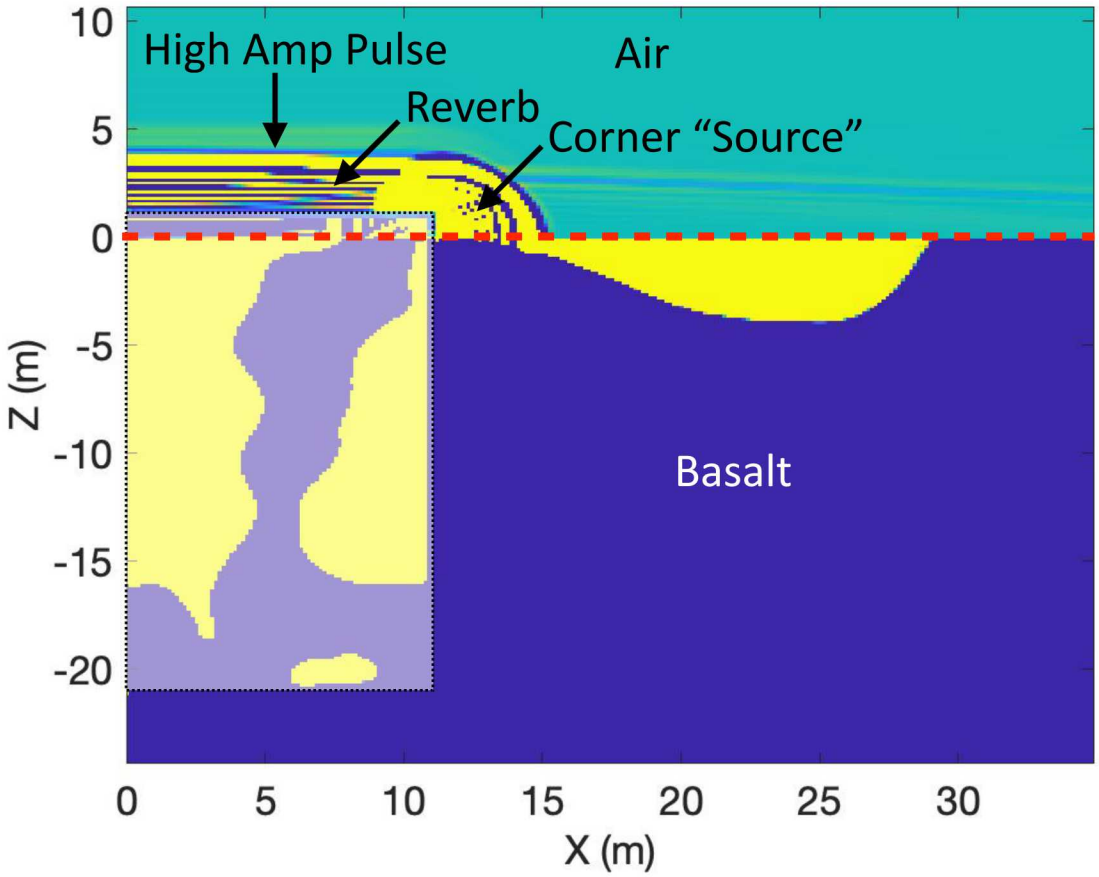

Figure 2-2: Example of a poorly performing CTH-axiElasti coupling. This is a time snapshot of the pressure wavefield. Red dashed line indicates the air-earth interface; light shaded area is the CTH regime with the black dotted line denoting the location of TVBC.

"source" described first clearly separates the two regimes: to the left (small offset, x), a large amplitude initial acoustic pulse, and to the right (larger offset), a smaller amplitude acoustic pulse produced directly by axiElasti. It is important to recall that the entire explosive source is surrounded by the TVBC, so even at these larger offsets, the initial data to drive the axiElasti simulations still came from CTH. However, at these larger offsets, the CTH-axiElasti coupling occurs within the earth. axiElasti then propagates this wavefield through the earth and across the air-earth interface into the air as an acoustic wave. Finally, note the high frequency reverberation that trails the initial acoustic pulse directly above the CTH domain. This reverberation would not be expected and, indeed, at larger offsets, the axiElasti acoustic pulse lacks these trailing reverberations.

Multiple test cases were conducted where we varied specific aspects of the basic model setup. For each setup, we varied the CTH grid spacing, moved the CTH initial element boundaries relative to the air-earth interface, moved the air-earth boundary within the axiElasti 1-D model, and moved the tracer positions relative to both the air-earth interface and CTH element boundaries. We found that when the CTH element boundaries did not align with the air-earth interface, or where tracer points sat directly on a CTH element edge the same issues as described above would contaminate results. In these cases, mixed cells were present from the outset of the simulations or interpolated based on the tracer location. Also, the initial specific values of some of the CTH nonlinear parameters (Table

Table 2-1. Key CTH parameters used for the first two cases

Case No.	Domain size (m)	Mesh Resolution (cm)	Air-Earth Interface (cm)	Mixed Cell at Air-Rock Interface?	Basalt Parameters		
					Tensile Strength (MPa)	Initial Pressure (MPa)	Initial Density (kg/m^3)
1	$0 \le r \le 300$ $-300 \le z \le 200$	1.25	0	No	-14.5	4.22	2868
2	$0 \le r \le 300$ $-250 \le z \le 150$	1.25	0	No	-10.0	0.10	2868

2-1) for the basalt had a significant effect on the acoustic amplitude directly emanated from CTH into the air via the TVBC.

Table 2-1 lists a few of the key parameters for two of the CTH cases being discussed. For both cases, the mesh resolution is such that the air-earth interface is in distinctly separate cells (this is also shown in Figure 2-3 below). For the first case, we decided to initially pre-stress the ground to 4.22 MPa. However, this initial pressure in addition to the hydrostatic pressure, due the z-direction gravity, can potentially over-stress the ground material. It is worth noting that for all CTH runs, we initialize the air using a 0.1 MPa pressure and density of 1.225 kg/m^3. Clearly, this results in a pressure gradient at the air-earth interface that might be one source of the problem noted earlier. In the second case, the mesh resolution is the same as Case 1; however, we use the same initial pressure of 0.1 MPa (with gravitationally stable distribution) as that in air. Note that we initially chose a tensile strength of -14.5 MPa, based on the average range suggested by Schultz (1995). A value of -10 MPa for the tensile strength is what we used in our previous studies, where this value is still within the range recommended by Schultz (1995).

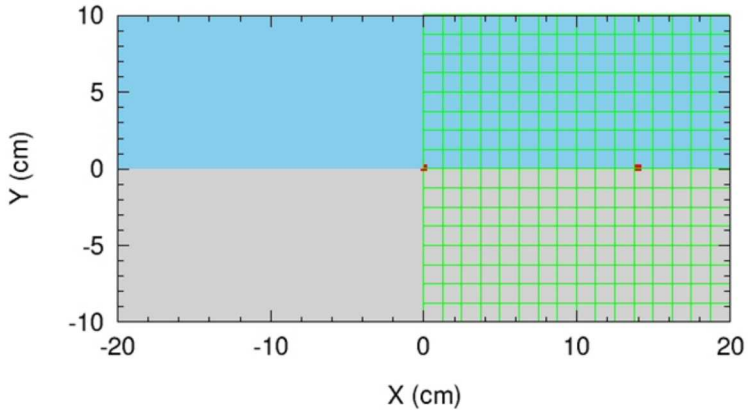

Figure 2-3: Close-up view of the CTH basic setup for Case #1 showing the materials (blue=air and grey=Earth) and the CTH mesh (green squares). Red dots depict two of the tracers. The air-Earth interface is located at Y = 0 cm, dividing the blue and grey regions.

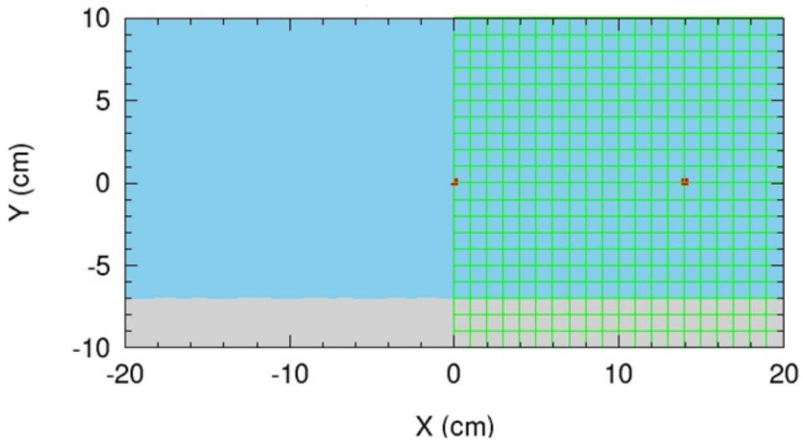

Figure 2-4: Close-up view of the CTH basic setup for Case #3 showing materials (blue=air and grey=Earth) and the CTH mesh (green squares). Red dots depict two of the tracers. The air-Earth interface is located at Y = -7 cm, dividing the blue and grey regions.

Table 2-2. Key CTH parameters used for Case #3, with the air-earth interface at z = -7 cm

Case No.	Domain size (m)	Mesh Resolution (cm)	Air-Earth Interface (cm)	Mixed Cell at Air-Rock Interface?	Basalt Parameters		
					Tensile Strength (MPa)	Initial Pressure (MPa)	Initial Density (kg/m^3)
3	$0 \le r \le 300$ $-250 \le z \le 150$	1.0	-7	No	-10.0	0.10	2868

Figure 2-3 depicts a close-up view of the CTH material with the mesh over-laid on top of the materials for the first two cases. Clearly, the air-earth interface is not in a mixed cell. However, tracers located at x[1]=z=0 and x=14 cm and z=0 can potentially experience the effects at the air-earth interface as they will sample from both air and earth cells.

[1] In 2DC CTH, x refers to the radial coordinate, r

2.3. Solution

We discovered four critical aspects of the modeling that had to be in place in order to obtain stable acoustic transmissions across the air-earth boundary from CTH to axiElasti:

1. The air-earth interface must be coincident with the CTH element boundaries, although as discussed above, this was already the case.
2. The tracer positions must not sample mixed cells via interpolation or directly mixed cells in CTH. In practice, we accomplished this by moving the air-earth interface down by 1/2 dh (i.e. 7 cm) in CTH and keeping the original tracer z-positions (see last bullet). Thus, for the model used here, the CTH air-earth interface was placed at z=-7 cm.
3. The proper set of nonlinear parameters must be used in the CTH simulation (see Table 2-2)
4. Tracer locations for the top of the TVBC box at z = 0 cm and z = +dh.

To illustrate the updated CTH problem setup, Figure 2-4 is the close-up view of the materials and the mesh near the air-earth interface. We can see that the air-earth interface is now at the z=-7 cm location and the tracers near the interface are now completely in the air.

Figure 2-5 shows the pressure history time series for the tracer at r = x = 0, for the three CTH cases discussed here. The upper most line (black) is the trace for Case #1 where the pressure starts at 4.22 MPa (basalt initial pressure) and then drops to ~2.7 MPa around 3 msec (roughly the time where the peak of the upward velocity, Vz, occurs—not shown here). The pressure then rises and stabilizes at ~3.25 MPa, although small amplitude oscillations are present through the rest of the simulations. We also see a similar pattern for Case #2 (red line), where the initial pressure drops from 0.1 MPa and goes into tension (reaches minimum at ~-1.8 MPa) and then rises again and stabilizes around ~-1.5 MPa (again small amplitude oscillations are present through the rest of the simulation). Finally, for Case #3 (blue line), the pressure remains at approximately 0.1 MPa, as it should, through the entire simulation (variations are too small to see at this scale). Keep in mind that the r=z=0 location, for Case #3 is entirely in the atmosphere. Nevertheless, the pressure variations for the first two cases are good indicators of the problem noted earlier, when CTH results are coupled with axiElasti code.

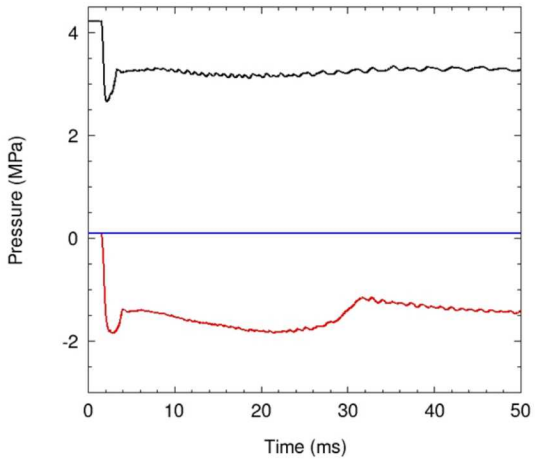

Figure 2-5: Comparison of pressure history for tracer at r=z=0 for Case #1 (black), Case #2 (red) and Case #3 (blue) lines. Case #3 appears flat at 0.1 MPa. Variations are present but are too small to visualize at this plot scale.

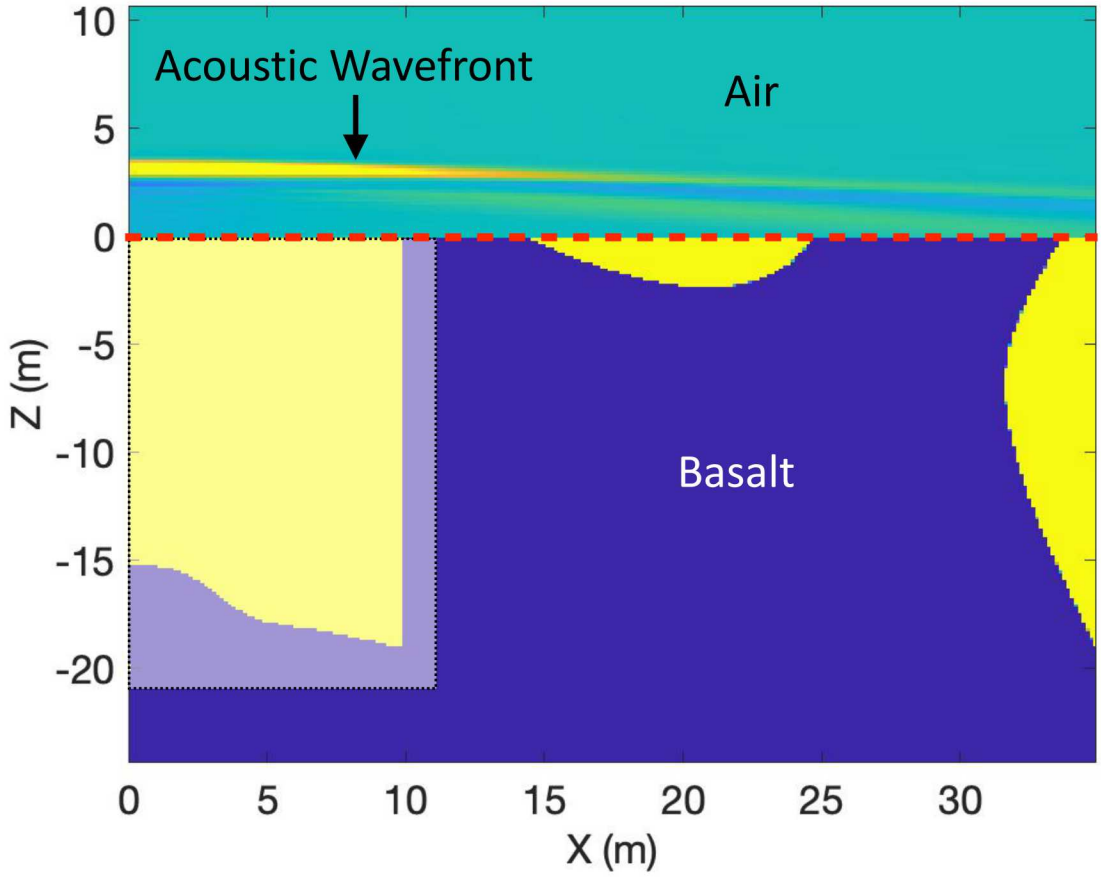

Figure 2-6: Example of a good performing CTH-axiElasti coupling. This is a time snapshot of the pressure wavefield. Red dashed line indicates the air-earth interface; light shaded area is the CTH regime with the black dotted line denoting the location of TVBC.

Because of the way axiElasti interprets 1-D velocity models, the air-earth interface is located at z=-7 cm in axiElasti as well. Thus, both CTH and axiElasti agree on the placement of the interface. It should also be noted that placing the top of the TVBC at z=0 cm and +dh are not the only possible placements. We found that as long as the top of the TVBC is located at z≥0 cm (basically completely in air) and has a thickness of dh, then no practical difference in simulation output is observed between the models. However, we are attempting to minimize the size of the TVBC so we choose the smallest z that is feasible. With these sets of restrictions, we obtain the results shown in Figure 2-6. Both the effects of the intersection of the TVBC and the air-earth interface (corner "source") and the very high amplitudes for the acoustic pulse above the CTH domain have been mitigated. A small amount of higher frequency reverberations do remain trailing the acoustic pulse immediately over the CTH domain, but these are greatly reduced in amplitude compared to the initial case and can be removed with filtering. Understanding the cause of the remaining small amount of reverberation is part of our continuing research. Overall, the pressure wavefield in the air appears continuous and smoothly varying as a function of X as one moves from the CTH-dominated region directly above the source to the axiElasti-dominated region beyond ~10 m. This means that the two algorithms are consistent across the air-earth interface, a minimum requirement for verification.

3. VERIFICATION AND TESTS

In this section we show verification and test cases for the implementation of the new nonlinear-linear coupling given in Section 2. The continuity of the pressure wavefield and the lack of extraneous "sources" in Figure 2-6 demonstrate that the two algorithms are consistent across the interface, a minimum requirement for verification, albeit a qualitative one. A more quantitative verification is comparison of source time function inversions using the new elastic-acoustic coupled version and the previous version that was purely elastic. If everything is consistent across the boundary then the estimated source time functions using the two algorithms should also be consistent with each other.

3.1. Model Setup

All the models given in this section, unless otherwise stated, are identical to the basic model setup given in Section 2.1 except that the TVBC is located at 10 m from the source. This means that the top of the TVBC zone has points at z = 0 cm and 14 cm, the bottom is at z = 20 m, and the radial side of the box is at roughly r = 10 m, each side with a thickness of 14 cm.

3.2. Source Inversion

All of these verification exercises will use linear full waveform seismic source time function inversion. The basic formulation of this technique is based on the premise that, in the linear elastic or acoustic regime, the observed waveforms are the earth's impulse response (Green's function) convolved with the source time function (e.g. Aki and Richards, 2000), or

$$d_{obs}(t) = G(t) * S(t) \tag{3-1}$$

where $d_{obs}(t)$ is the observed seismic waveform as a function of time, $G(t)$ is the impulse response of a given source type (e.g. explosion, force, moment tensor component), and $S(t)$ is the source time function for the source. In this report, the "observed" data will come from CTH coupled to axiElasti, whereas the Green's functions will be computed entirely by axiElasti using an impulse source in both time and space located at z = -10 m, r = 0 m.

In the frequency domain, the convolution becomes multiplication:

$$d_{obs}(f) = G(f)S(f) \tag{3-2}$$

This equation can be inverted to solve for an unknown source time function given the observed data and the impulse response

$$S(f) = \frac{d_{obs}(f)}{G(f)} \tag{3-3}$$

For multiple observations and corresponding Green's functions, Equation 3-2 can be converted to a linear system of equations that can be solved for a single or multiple source time functions. These equations can be solved frequency by frequency:

$$\mathbf{d_{obs}} = \mathbf{GS} \tag{3-4}$$

where $\mathbf{d_{obs}}$ is a n x 1 matrix of n observations at a given frequency, $\mathbf{G}$ is a n x m matrix of the Green's function responses at that frequency for m sources, and $\mathbf{S}$ is an m x 1 matrix of the m source responses at that frequency. Typical matrix inversion techniques will produce the sought-after source response given Green's functions and observations at each frequency, and then inverse Fourier transforming will yield source time functions. See Poppeliers et al. (2020) for a more in-depth explanation of the source inversion problem.

3.3. Baseline: Source Inversion with Elastic-Only Receivers

This is the baseline case that was presented in Preston et al. (2019). The baseline case uses the same model setup given in Section 3.1 for the CTH domain except that there is no top to the TVBC box, only the bottom and side. The reason for this is that the axiElasti model has no air layer; thus, no transmission into the air is required. The top of the axiElasti model is at z = 0 m and is set to an explicit stress-free surface boundary condition. This condition approximates an air-earth boundary by applying the boundary condition $\sigma_{rz} = \sigma_{zz} = 0$ at z = 0 m (see Preston (2017) for more details on this boundary condition). This boundary condition is useful and quite accurate when the only thing one desires is the elastic earth response, and air-earth interactions and acoustic transmission are not required. Another important difference between this purely elastic model and the basic setup is that a 2000 Hz low pass filter was used to process the TVBC responses before input into axiElasti since the higher wave speeds present in the purely elastic model can support higher frequencies at the model node spacing of dh = 14 cm.

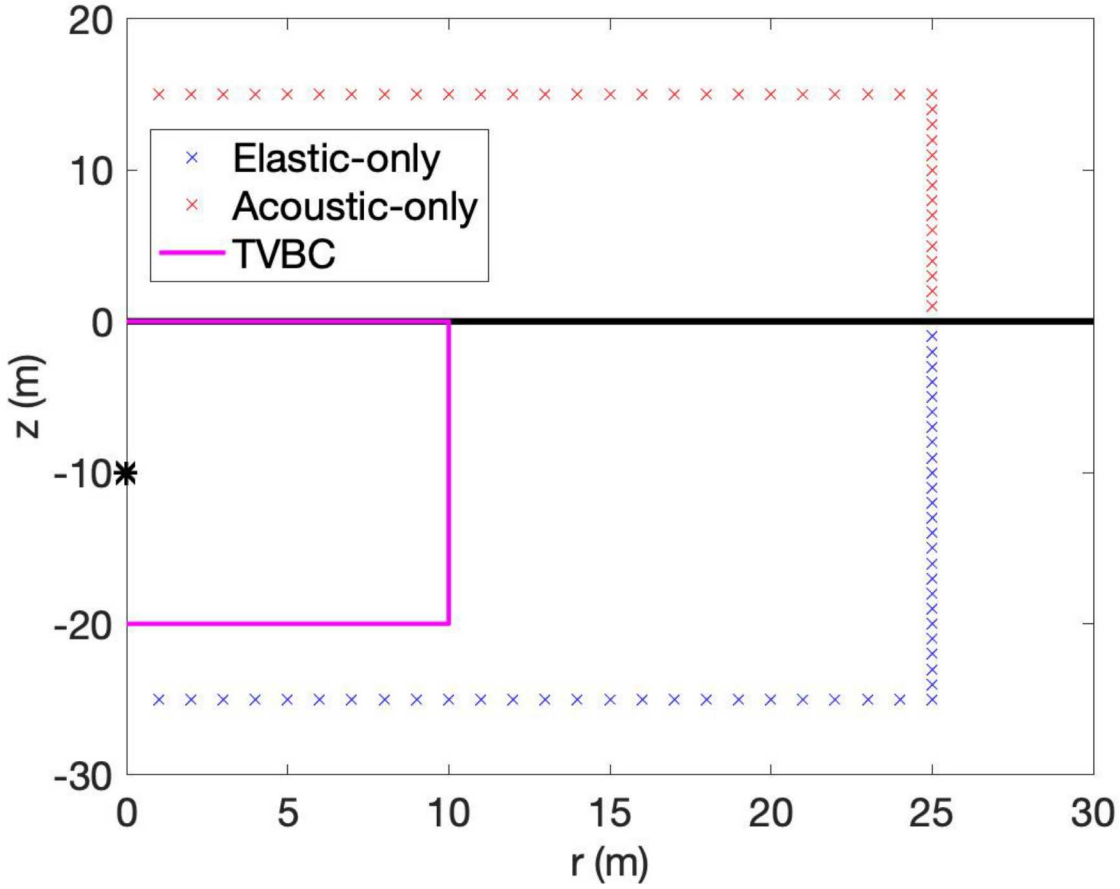

Figure 3-1: Velocity receiver locations used in the Baseline elastic (blue x's) and pressure receiver locations (red x's) used in the new code. Magenta box denotes the nonlinear-linear TVBC coupling box. Black line indicates the air-earth interface. The elastic-only receivers are the only receivers used in the Baseline simulation (Section 3.3); the acoustic-only receivers are the only receivers used in the verification of the new coupling interface in Section 3.4.

In this case, radial and vertical velocity receivers are placed within axiElasti in order to surround the source below and at range (blue x's in Figure 3-1). Again, no receivers are placed above the CTH domain since there is no air layer. Only the velocity receiver components are used in the inversion for the optimal linear source time function. An explosion (isotropic moment tensor) is assumed for the source type; thus, there is only one source time function output from this inversion. The resulting source time function, using only elastic velocity receivers within the solid earth, are shown in Figure 3-2 as the blue line.

3.4. Source Inversion with Acoustic-Only Receivers

Here we compare the source time function obtained by inverting only pressure receivers within the air using the new algorithm with the elastic-only inversion from the previous subsection. The model setup for this case is exactly as described in Section 3.1. The model and TVBC completely surround the source on all sides. However, for this case the receivers used for the inversion are located completely in air and only pressure receivers are used (red x's in Figure 3-1). Again, an explosion source is assumed, resulting in a single source time function from the inversion (red in Figure 3-2).

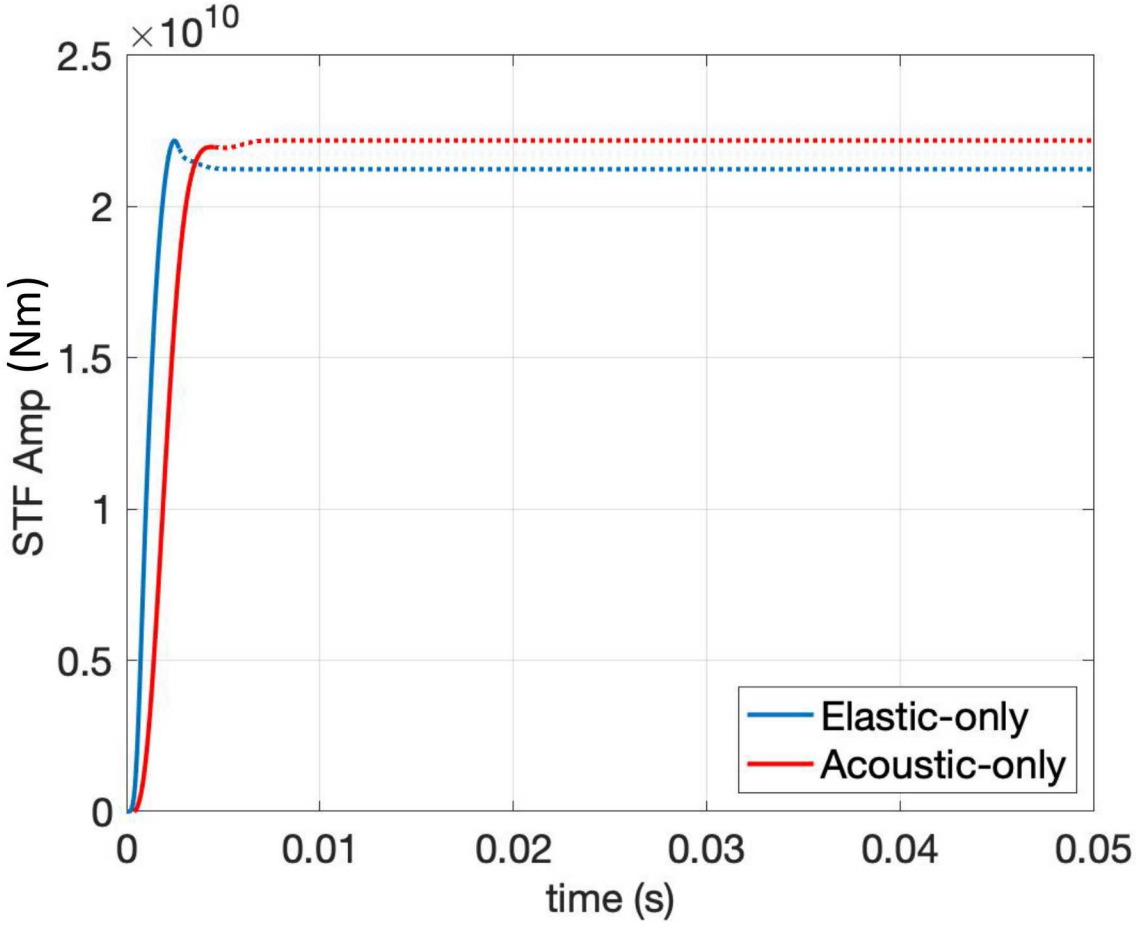

Figure 3-2: Comparison of the source time function inversion results for the Baseline elastic-only (Section 3.3) and acoustic-only (Section 3.4) cases. Dashed portions uncertain.

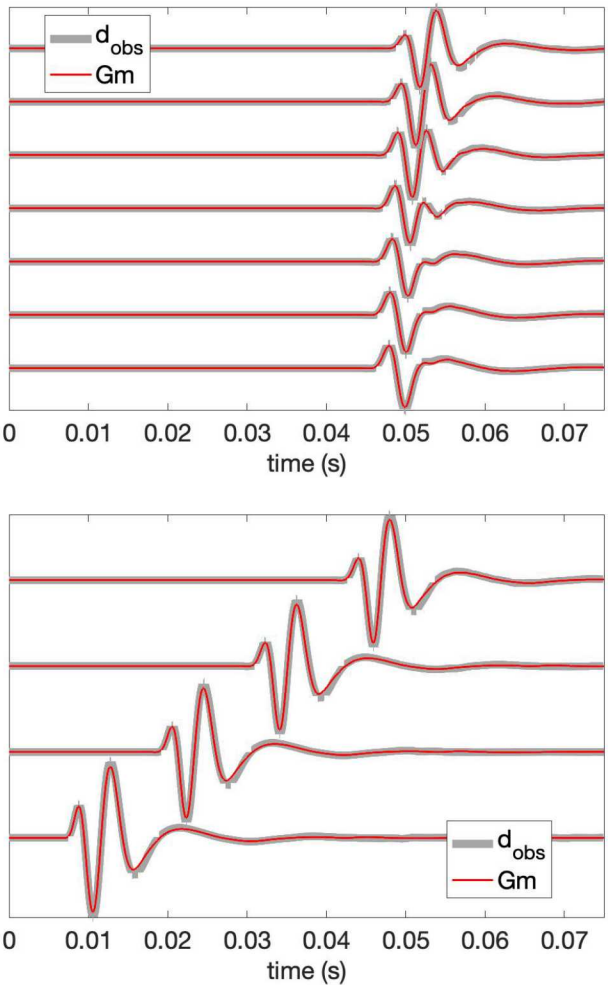

Figure 3-3: Comparison of observed data (d_{obs}) derived from CTH to modeled (Gm) using the linear source time function in Figure 3-2 acoustic-only for pressure receivers in the acoustic-only case at z = 15 m (top) and r = 25 m (bottom), both completely in air. Each trace is scaled to the maximum amplitude of d_{obs} for that trace.

The two inversion results are very similar with nearly identical peak amplitudes. This is despite some differences in the respective pre-processing and inversions as have been mentioned. To reiterate, the elastic-only case uses an approximate boundary condition at the interface, namely the stress-free surface, compared to a coupling that allows the physical equations to propagate energy across the interface. Secondly, the elastic-only TVBC input is low-pass filtered to 2000 Hz, whereas the acoustic-only results use a 240 Hz low pass filter. This latter difference is clearly apparent in the more gentle (lower frequency) rise to the peak source amplitude for the acoustic-only source time function relative to the elastic-only source estimate. Given the close agreement of these two results based on two datasets, one completely contained within the elastic earth, the other using the coupled air-earth nonlinear-linear interface, indicate that the new algorithm is consistent both qualitatively and quantitatively with the original elastic-only version of the code.

Figure 3-3 demonstrates the high-quality fit of the CTH-derived observed data using a purely linear source time function. The average cross-correlation coefficient between the observed and modeled data is 0.996.

3.5. Combined Elastic and Acoustic Inversion

To further demonstrate the effectiveness and consistency of the new air-earth interface, we show two additional cases, each using receivers both in the air and earth in a simultaneous inversion. Both cases use the setup as described in Section 3.1. They differ in their respective receiver geometries.

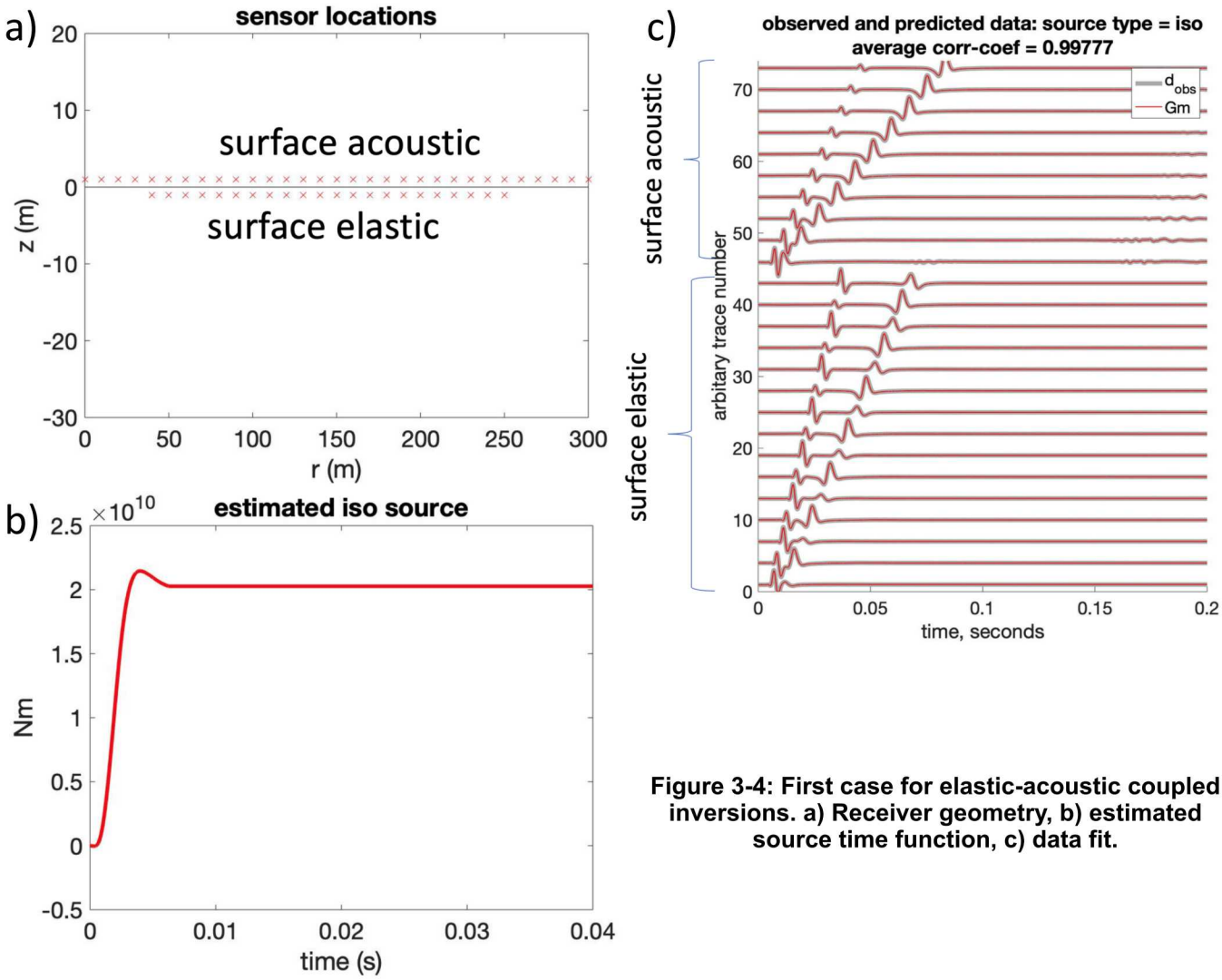

Figure 3-4: First case for elastic-acoustic coupled inversions. a) Receiver geometry, b) estimated source time function, c) data fit.

The first case uses a fairly realistic arrangement of 2-C (radial and vertical) velocity and pressure receivers with the pressure receivers located just above the surface representing acoustic sensors and a set of velocity receivers shallowly buried within the earth (Figure 3-4a). A joint inversion of the elastic velocity receivers with the acoustic pressure receivers yield the explosion source time function shown in Figure 3-4b. Note the similar shape and magnitude of this source time function to those obtained in Figure 3-2, another indication that the nonlinear-linear interface is behaving consistently within expectations. The fit to the CTH-derived observed data is excellent for both seismic and acoustic receivers, further demonstrating the accuracy of the interface (Figure 3-4c).

In addition to the surface acoustic and elastic receivers present in the first case, the second case also includes borehole seismic (velocity receivers in a vertical line as in a borehole) and airborne acoustic sensors (pressure receivers suspended above the surface as in a balloon) (Figure 3-5a). This represents a more idealized receiver geometry. The joint inversion of these elastic and acoustic sensors produces the explosion source time function shown in Figure 3-5b. Again, the similarity to results in the prior subsections demonstrates the validity of the new coupling method both above and below the air-earth interface. Figure 3-5c also shows that seismic receivers at depth and acoustic receivers to the side and above the TVBC are all consistent with each other and are well-fit by the linear source time function estimate.

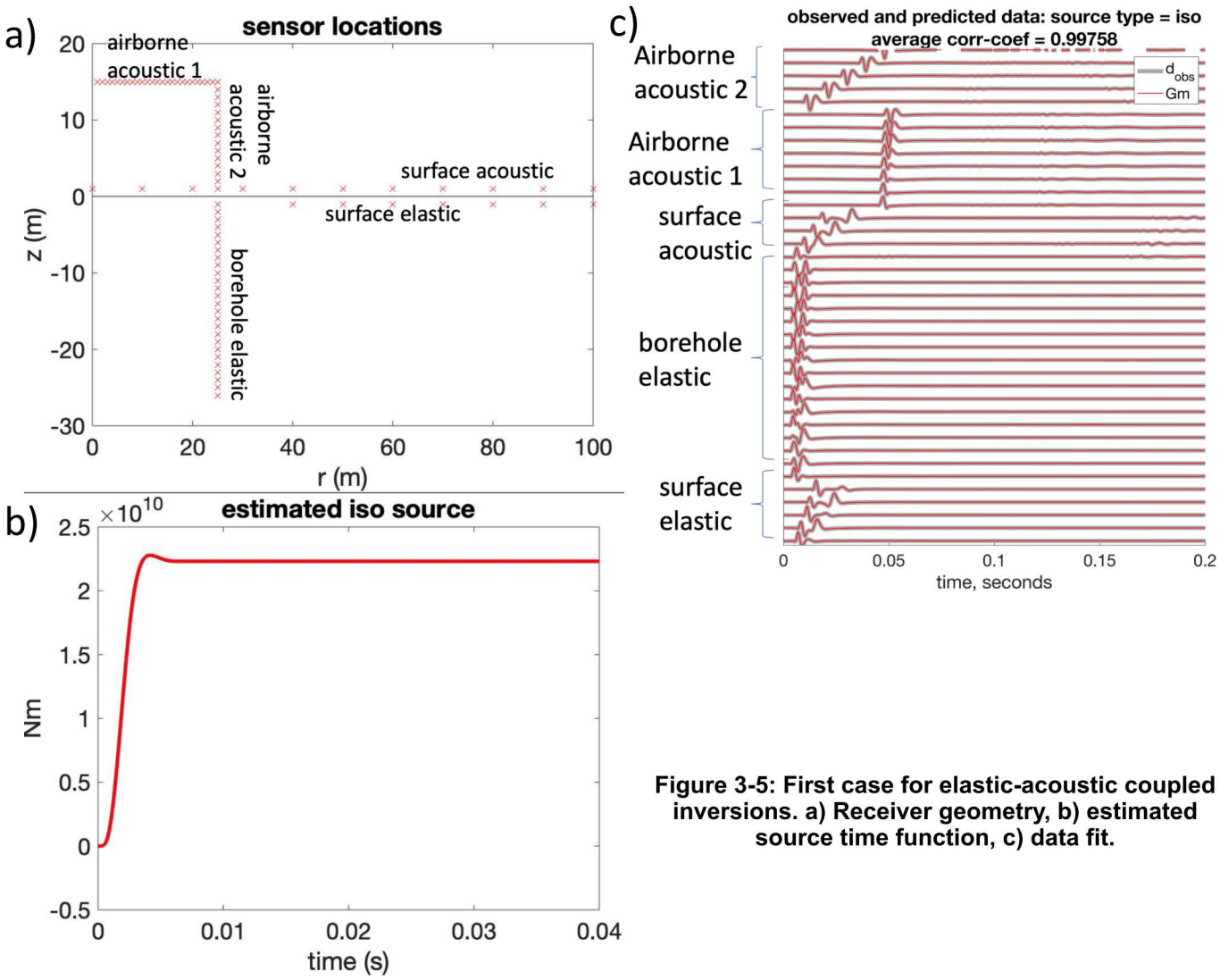

Figure 3-5: First case for elastic-acoustic coupled inversions. a) Receiver geometry, b) estimated source time function, c) data fit.

3.6. Inversion Using Other Materials

The previous sections used basalt as the earth material in the air-earth coupling. In addition to basalt, we also evaluate two other materials: salt and wet tuff. We applied the same setup as given in Section 3.1 except for the change in earth materials. For salt we used seslan number 7282 (Kerley and Christian-Frear 1993) for CTH and Vp=4620 m/s, Vs=2667 m/s, and density 2140 kg/m^3 for the axiElasti runs. For wet tuff we used seslan number 7120 (Kerley and Christian-Frear 1993) for the CTH run and Vp=3278 m/s, Vs=1982 m/s, and density 1950 kg/m^3 in axiElasti. We used the same parameters as stated in Table 2-2 except a 1.5 cm mesh resolution was used in addition to the proper density for the material. A more coarse CTH mesh resolution was used to investigate how sensitive the coupling interface is to the mesh resolution and the resulting change in numerical accuracy. Figure 3-6 compares the elastic-only solutions and acoustic-only solutions for salt and wet tuff analogous to Section 3-4 (and repeats basalt for reference). Even with the lower CTH mesh resolution, both the elastic-only and acoustic-only source time function inversions yield very similar shapes and peaks with the same caveats as discussed in Section 3.4.

An interesting side note is the comparison of the peak amplitudes of the source time functions from the three different materials (Figure 3-6). The peak amplitude for basalt is approximately 2e10

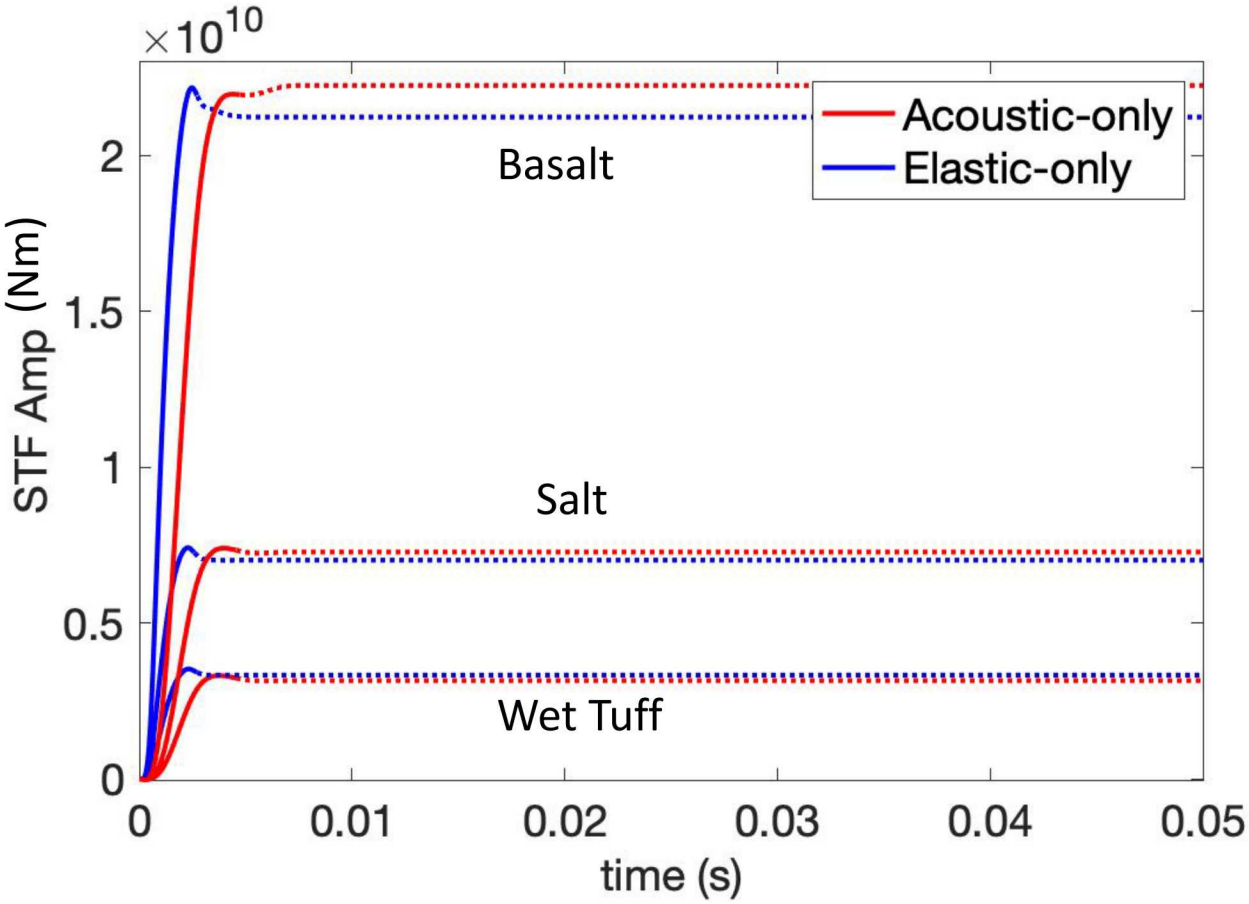

Figure 3-6: Comparison of the source time function inversion results for the Baseline elastic-only (see Section 3.3) and acoustic-only (see Section 3.4) cases for basalt, salt, and wet tuff as materials. Dashed portions uncertain.

Nm, for salt 7e9 Nm, and for wet tuff it is 3e9 Nm. Recall the explosive energy (4.5 kg TNT) is the same in all three cases; only the earth material varies. As mentioned in Preston et al. (2019) the peak amplitude scales as roughly the seismic impedance (density times Vp) of the material. Thus, the linear seismic source time function one obtains is material dependent, not just source-energy dependent.

4. CONCLUSION

We have detailed the method we found that stably and accurately couple the nonlinear shock physics code CTH to the linear seismo-acoustic algorithm axiElasti. CTH drives the nonlinear motions near the source up to and including the earth's surface and directly adjacent air. From there axiElasti uses this CTH-derived output to drive TVBC's to propagate elastic and acoustic waves into the far field. We find that properly aligned locations for TVBC points, the air-earth interface, and CTH cell boundaries are critical for accurate transmission across this high-contrast boundary. In particular, these locations must be such that there is no sampling or mixing of air and earth material in CTH cells. Furthermore, a proper set of CTH nonlinear material properties had to be used to obtain accurate results.

In this report, we demonstrate the validity and accuracy of the new methodology both qualitatively and quantitatively. Continuity of the acoustic wavefield from the region of the model dominated by direct CTH transmission into air to that dominated by axiElasti, where the CTH coupling occurs primarily within the solid earth, qualitatively confirm the effectiveness of the new technique. We quantitatively verify the new method with several comparisons with results from source time function inversions. First we verified that we obtain nearly identical results for source time functions inverted from elastic-only recordings in a model without any air-earth boundary and those using the new method with acoustic-only receivers. Secondly, we substantiated this by showing again nearly identical results when using two different geometries of elastic and acoustic receivers in a joint inversion. Furthermore, we tested the air-earth boundary with three different earth materials: basalt, salt, and wet tuff. In all cases, the inverted source time functions reproduce the data derived from CTH extremely well. This, in turn, demonstrates that at least for the deeply-buried explosion source used in our modeling, that a linear source model can accurately and effectively replicate waveforms from a nonlinear source. An interesting side note that deserves further investigation is that the amplitudes of the resultant linear source models scale roughly according to the seismic impedance of the earth material for a fixed source energy. Although we evaluated the interface with three materials, it is possible that some nonlinear material properties may need to be adjusted for other materials.

Additional work in the future will focus on a more nuanced analysis of the TVBC air-earth interface described in this report. These include a better understanding of the remaining low amplitude, high frequency reverberations that follow the primary acoustic pulse above the source and of the effects of CTH material properties (e.g. strength model) on the seismo-acoustic response. We will also be pursuing additional research to clarify how inhomogeneous earth materials affect this coupling.

REFERENCES

1. Aki, K., and P.G. Richards (2002). *Quantitative Seismology*, Second Edition, University Science Books, Sausalito, CA.
2. Kerley, G.I. and T.L. Christian-Frear (1993). *Sandia Equation of State Data Base:* seslan *File*, SAND93-1206, Sandia National Laboratories, Albuquerque, NM.
3. Poppeliers, C., Wheeler, L.B., and L. Preston (2020). The Effects of Atmospheric Models on the Estimation of Infrasonic Source Functions at the Source Physics Experiment, *Bull. Seis. Soc. Am.* **110**(3), 998-1010.
4. Preston, L.A. (2017). *Nonlinear to Linear Elastic Code Coupling in 2-D Axisymmetric Media*, SAND2017-8848, Sandia National Laboratories, Albuquerque, NM.
5. Preston, L.A., D.F. Aldridge, and N.P. Symons (2008). Finite-Difference Modeling of 3D Seismic Wave Propagation in High-Contrast Media, Soc. Expl. Geophys. 2008 Annual Meeting Extended Abstracts.
6. Preston, L., M. Eliassi, A. Gullerud, and C. Poppeliers (2019). Nonlinear Effects on Linear Seismic Source Inversions from Simulations of Underground Chemical Explosions, Seism. Soc. Am. 2019 Annual Meeting Abstracts.
7. Schmitt, G., D.A. Crawford, E.N. Harstad, D.M. Hensinger, and K.P. Ruggirello, (2017). *CTH User's Manual and Input Instructions, Version 12.0, CTH Development Projects*, Sandia National Laboratories, Albuquerque, NM, April 20, 2017 (OUO).
8. Schultz, R.A. (1995). Limits on Strength and Deformation Properties of Jointed Basaltic Rock Masses, *Rock Mech. Rock Engng.* **28**(1), 1-15.

DISTRIBUTION

Email—Internal

Name	Org.	Sandia Email Address
Scott Broome	8864	stbroom@sandia.gov
Technical Library	01977	sanddocs@sandia.gov

This page left blank

This page left blank

Sandia National Laboratories

Sandia National Laboratories is a multimission laboratory managed and operated by National Technology & Engineering Solutions of Sandia LLC, a wholly owned subsidiary of Honeywell International Inc. for the U.S. Department of Energy's National Nuclear Security Administration under contract DE-NA0003525.